RADIOTHERAPY VOLUME DELINEATION USING DYNAMIC [^{18}F]-FDG PET/CT IMAGING IN PATIENTS WITH OROPHARYNGEAL CANCER – A PILOT STUDY

Antti Silvoniemi, M.D. (corresponding author)
Turku University Hospital
Department of Otorhinolaryngology – Head and Neck Surgery
P.O. BOX 52
FI-20521 Turku
Finland
e-mail: anmisi@utu.fi
phone number: +358405190633

Mueez U Din, M.Sc.
Turku PET Centre
P.O. BOX 52
FI-20521 Turku
Finland

Sami Suilamo, M.Sc.
Turku University Hospital
Department of Oncology and Radiotherapy
Department of Medical Physics
P.O. BOX 52
FI-20521 Turku
Finland

Tony Shepherd, PhD
Turku University Hospital
Department of Oncology and Radiotherapy
P.O. BOX 52
FI-20521 Turku
Finland

Heikki Minn, M.D. Professor
Turku University Hospital
Department of Oncology and Radiotherapy
P.O. BOX 52
FI-20521 Turku
Finland

Abstract

Purpose: Delineation of gross tumour volume in 3D is a critical step in the radiotherapy (RT) treatment planning for oropharyngeal cancer (OPC). Static [^{18}F]-FDG PET/CT imaging has been suggested as a method to improve the reproducibility of tumour delineation, but it suffers from low specificity. We undertook this pilot study in which dynamic features in time-activity curves (TACs) of [^{18}F]-FDG PET/CT-images were applied to help the discrimination of tumour from inflammation and adjacent normal tissue. **Methods:** Five patients with OPC underwent dynamic [^{18}F]-FDG PET/CT- imaging in treatment position. Voxel-by-voxel analysis was performed to evaluate seven dynamic features developed with the knowledge of differences in glucose metabolism in different tissue types and visual inspection of TACs. The Gaussian mixture model and K-means algorithms were used to evaluate the performance of the dynamic features in discriminating tumour voxels compared to the performance of standardized uptake values obtained from static imaging. **Results:** Some dynamic features showed a trend towards discrimination of different metabolic areas but lack of consistency means that clinical application is not recommended based on these results alone. **Conclusions:** Impact of inflammatory tissue remains a problem for volume delineation in RT of OPC but a simple dynamic imaging protocol proved practicable and enabled simple data analysis techniques that show promise for complementing the information in static uptake values**.**

Keywords: oropharyngeal cancer, PET/CT, [^{18}F]-FDG, dynamic PET/CT-imaging, contouring, radiotherapy

Introduction

Hybrid positron emission tomography computed tomography (PET/CT) imaging with [^{18}F]-fluorodeoxyglucose ([^{18}F]-FDG) is commonly used in the management of patients with oropharyngeal cancer (OPC). Concurrent chemoradiotherapy (CRT) is the preferred treatment modality for locally advanced OPC, and approximately 70-80% of patients can be expected to achieve local control with platinum-based drugs and conformal irradiation techniques [1].

Although the overall survival of patients with OPC has improved since the introduction of CRT, the treatment frequently causes remarkable and even life-long adverse effects [2,3], motivating research into better personalization of treatment plans. First, the improved accuracy of gross tumour volume determination utilizing [^{18}F]-FDG PET/CT may be beneficial in limiting the dose in sensitive normal tissues such as salivary glands, spinal cord and mandible [4,5]. Second, the improvement in survival has been paralleled with the rising incidence of human papilloma virus (HPV) infection, which accounts for more than two thirds of all OPCs in the Western world [6,7,8]. Patients with HPV-positive OPC have better prognoses compared to HPV-negative patients [8,9], and some of the HPV-positive patients would survive without undergoing the most intensified treatment protocols [10]. This observation has prompted discussion about the de-intensification of treatment in individual patients [11], but this remains an experimental approach and de-intensified protocols require rigorous imaging applications given that cervical lymph node metastases are extremely common in patients with HPV-positive OPC.

In planning of RT, one major challenge is the task of reliably delineating malignant tissues in 3D using different datasets such as PET/CT or magnetic resonance imaging. The limited specificity of [^{18}F]-FDG to differentiate between neoplastic and inflammatory tissue is a well-recognized problem that stems from the fact that all cells with increased rate of intracellular glucose consumption are [^{18}F]-FDG-avid and present as hot spots in PET images [12]. Static [^{18}F]-FDG-PET/CT-imaging and semiquantitative tracer uptake analysis using standardized uptake value (SUV) is a widely applied technology in oncology, but the method is suboptimal in the identification of malignant tissue for delineation of RT targets. To overcome the limitations of a static approach in differentiation between cancer and inflammation, the images can be further analyzed by taking into account the temporal dimension of tracer uptake [13]. Probably the most common investigated application in this field is dual-time point imaging. However, this relatively robust and reproducible method has not totally fulfilled expectations in patients with head and neck cancer [14].

Motivated by the limitations of static and dual-time point image analysis, we hypothesized that different tissue types may show differences in the temporal pattern of [^{18}F]-FDG uptake better identifiable by more advanced analysis of more temporally detailed dynamic images. To address this hypothesis we tested several features, calculated from PET activity curves of 22 time-points, for their ability to discriminate different metabolic areas in dynamic [^{18}F]-FDG PET/CT-images of patients with OPC undergoing CRT. We further hypothesized that knowledge of the pattern of these features derived from tumour and inflammatory tissues would be useful for the delineation of RT volumes.

Methods

Patients

The study was conducted at Turku University Hospital, which is a tertiary academic center in Southwestern Finland. Five patients with newly diagnosed and untreated OPC were enrolled in the study. The median age of the patients was 59 years (range 58-65), and all patients were in good or moderate general health condition (Zubrod performance status score 1-2). The characteristics of the patients are presented in Table 1. Informed consent was obtained from all individual participants included in the study. All procedures performed in the study involving human participants were in accordance with the 1964 Helsinki Declaration and its later amendments. The study protocol was accepted by the Ethics Committee of the Hospital District of Southwest Finland. The patients underwent standard biopsy procedures (either tonsillectomy or tissue biopsy during hypopharyngoscopy depending on the site of the tumour) before PET/CT-imaging was performed. The median time from biopsy to scan was 21 days (range 16-23 days). Standard immunohistochemical staining of the tissue specimen using p16 antigen test was performed to determine the human papilloma virus (HPV) status [15].

The pre-study management included standard dentist´s evaluation, which consisted of an oral hygiene plan, extraction of decayed teeth, and management of oral chronic infections when necessary. All procedures were depicted in detail in the dental report, available for investigators, defining volumes of interest for RT and study protocol (see below).

PET/CT Device and image reconstruction

All scans were performed with a hybrid Discovery VCT PET/CT-scanner (General Electric Medical Systems, Milwaukee, WI, USA), which combines a helical 64 slice CT scanner and a PET tomography with bismuth germinate oxide crystals arranged in 24 rings, yielding 47 transverse slices of 3.27 mm slice thickness. The PET imaging field of view was 70 cm in diameter and 15 cm in axial length. Image reconstruction was performed with an iterative VUE Point Fx method (GE Healthcare, 2011) with 2 iterations and 24 subsets. A reconstruction matrix of 192x192 was used.

Imaging protocol

The PET/CT acquisition protocol was designed both for the study purposes and for the planning of the standard RT. The patients fasted for at least 4 hours before the scan was performed. Then the patient was positioned supine, arms down on the scanner couch with a flat table and a thermoplastic mask for the immobilization. The scanner landmarks were set to the predefined marks on the mask. A CT scan from the neck region was acquired, and after that, the injection of [^{18}F]-FDG was administered intravenously. At the same time as the injection, the dynamic PET scan was started. During the first 30 minutes, dynamic PET data from the neck region was acquired (0-30 minutes divided in 20 frames, please see Fig. 1 for details). After that, the patients were allowed to rest outside the scanner before the second imaging session began.

The second imaging session started with a whole-body CT scan for the treatment planning purposes followed by the standard diagnostic whole-body PET scan containing two bed positions from the neck region (4 minutes per bed position) and two bed positions from the lower part of the body (2 minutes per bed position). Finally, one frame of the PET data from neck region (one bed position, four minutes frame) was acquired. In total, the PET data contained 22 frames. The imaging data of

the 21st frame was used in order to determine the uptake value in the form of static parameter SUV. The scanning protocol is presented in detail in Fig. 1.

Image analysis

Volumes of interest (VOIs) were determined on the co-registered PET/CT images. The primary tumours and all metastatic lymph nodes were contoured manually by a qualified radiation oncologist on the images from the 21st frame. Identification of primary tumours was based on detection of an FDG-avid lesion in an area with a history of positive biopsy, excluding physiological tracer uptake, and, in the case of metastases, detection of a FDG positive lesion in the neck where the overlaying lymph node could be seen on anatomical CT. The largest metastatic lymph node when available was chosen for further analysis.

Healthy tissue surrounding a primary tumour VOI (Gross Tumour Volume) was defined using a voxel threshold method: First, a box-shaped VOI was defined around the irregular-shaped tumour VOI, then tumour voxels (according to the manually contoured tumour VOI) were subtracted from this box-shaped VOI leaving behind the healthy tissue voxels. The voxels belonging to any other nearby VOI contour (e.g. inflammation) were also excluded in the rare cases where they fell inside the same box-shaped VOI.

In addition to tumours and metastases, VOIs representing inflammatory lesion(s) in the mandible or other parts of the oral cavity were drawn manually on the PET/CT images, paying specific attention to the written report of all dental procedures. All the patients had at least one inflammatory lesion due to extraction of decayed teeth, which was feasible for further analysis of PET data. All the VOIs that were drawn on the PET/CT images from the 21st frame were rigidly registered with the corresponding PET/CT images from the first part of the imaging session (frames nr 1-20).

Evaluation of dynamic features in the distinction of different tissue types

Time-activity curves (TACs) were generated for every single voxel of the predefined VOIs. A number of dynamic features were developed for voxel classification. Design of these features was based on visual inspection of TACs and assumptions based on knowledge of glucose transport mechanisms. The dynamic features (D1-D7) are defined in Table 2 and described in detail in the master thesis of Mueez U Din [16]. SUV and all dynamic features were calculated for each of the voxels from the predefined VOIs. These predefined VOIs provided the best available ground-truth for labelling voxels according to tissue type.

Two classification algorithms Gaussian mixture model (GMM) and K-means were used to evaluate performance of the dynamic features and SUV in the distinction of different tissue types. The classification and performance evaluation were implemented in the programming software Matlab (Version: R2006b). GMM code was adapted from open-source code in Simulink´s on-line archive of open-source libraries (Matlab Central – File exchange, 2013), and K-means is a built-in function of the Matlab statistical toolbox package. Starting with 4 tissue types: primary tumour, inflammation, metastatic lymph node and healthy tissue surrounding the primary tumour, we performed 4 binary classification experiments that discriminated (i) tumour vs. inflammatory tissue, (ii) tumour vs. healthy tissue, (iii) tumour vs. metastatic lymph node and (iv) inflammatory tissue vs. metastatic lymph node.

In each binary classification, a mixture of unlabeled data from two different tissue types was input to a classification algorithm, which was set up to divide the data into two classes based on the evaluated dynamic feature or SUV. Each algorithm produced a label according to whether the voxel belonged to the positive class (e.g. primary tumour) or negative class (e.g. healthy tissue). These labels were compared to the ground-truth labels in order to calculate specificity and sensitivity of the dynamic features and SUV. For the K-Means algorithm, the specificity and sensitivity values were presented separately whereas for the GMM algorithm, receiver operating characteristics (ROC) analysis was performed. The area under the curve (AUC_{ROC}) is a combined measure of sensitivity and specificity and was used as performance metric for the GMM algorithm.

Finally, sensitivity and specificity of the dynamic features were compared with those of the static parameter SUV. For comparison between the performance of a dynamic feature and SUV, Wilcoxon rank-sum test was used to investigate the statistical significance of differences. The non-parametric test was chosen because of the low number of patients.

Treatment of oropharyngeal cancer

After PET/CT imaging, all patients received standard treatment assigned for them in a multi-disciplinary tumour board. It consisted of intensity-modulated RT to the primary tumour and bilateral neck applying international guidelines [17]. Irradiation was combined with concurrent weekly cisplatin (40 mg/m^2) over six weeks. One patient with sensorineural hearing loss (nr 4) received weekly cetuximab (250 mg/m^2) instead of cisplatin [18]. Patients nrs 2,3, and 4 also underwent neck dissection as a first-line surgery 3 weeks after completion of CRT. All patients received post-treatment [^{18}F]-FDG PET/CT scan three months after CRT. Patients with residual or recurrent disease received additional chemotherapy either alone or combined with surgery.

Results

General evaluation of time-activity curves and tissue uptake

The patients (nrs 1-3) with tonsillar carcinoma had lower [^{18}F]-FDG uptake in their primary tumours compared to the two patients (nrs 4-5) with non-tonsillar carcinoma. Furthermore, the tonsillar carcinoma patients had higher tracer uptake in the inflammatory regions compared to the uptake of the primary tumour. Visual inspection revealed that the patients with tonsillar carcinoma also had a different shape of the TAC of the primary tumour compared to the non-tonsillar carcinoma patients (Fig. 2 and Fig. 3). The mean SUVs from all VOIs are presented in Table 3. The median SUV of the metastatic lymph nodes was lower than that of the inflammatory regions in the whole study population (Table 3). An example of PET/CT images is presented in Fig. 4.

Discriminating primary tumour from inflammation

The performance of the two classification algorithms in discriminating primary tumour from inflammatory voxels is presented in Table 4. Using the GMM algorithm, dynamic feature D3 showed slightly better performance compared to SUV, but the difference was not statistically significant ($p= 0.82$). Among non-tonsillar carcinoma patients, D1 and D6 provided some superior ability compared to SUV, although these differences were not significant ($p= 0.33$ for both of them).

The test with K-means algorithm provided slightly different results (Table 4). The feature D3 provided a lower sensitivity compared to the SUV in the whole patient population, and D6 was not superior compared to the SUV among non-tonsillar carcinoma patients.

Discriminating primary tumour from surrounding healthy tissue
The dynamic features were also utilized to discriminate the voxels of primary tumours from the surrounding healthy tissue. Both GMM and K-means clustering algorithms were used in these calculations. The results are shown in Table 4, and none of the dynamic features was found to be superior to SUV.

Discriminating a metastatic lymph node from inflammation and from primary tumour
The dynamic features did not provide superior performance compared to SUV in the distinction between metastatic lymph node and inflammation. Instead, the analysis between metastatic lymph nodes and primary tumours revealed that, to some extent, D5 showed superior sensitivity and specificity compared to SUV, when K-means algorithm was used. The results of both two comparisons with GMM and K-means algorithms are presented in Table 4.

Discussion

[^{18}F]-FDG PET/CT has revolutionized the imaging of several types of malignant tumours [19]. Nonetheless, the low specificity of [^{18}F]-FDG uptake in the identification of malignant tissue, mainly due to increased glucose metabolism of inflammatory tissue, remains a remarkable challenge [12]. This problem affects not only diagnostic imaging but also the delineation of RT volumes in complex anatomic regions such as the head and neck area. Bearing this difficulty in mind, we overtook the current study and evaluated the novel dynamic features of [^{18}F]-FDG uptake in patients with head and neck cancer scheduled for CRT. We felt that dynamic imaging in treatment position might be helpful in the distinction of different tissue types compared to the standard approach, thus assisting in the contouring of tumours and minimizing the excess irradiation of normal tissues.

Some differential features in the glucose metabolism and transport of neoplastic and non-neoplastic tissues can potentially be discernible in dynamic imaging. Of these, the expression of glucose transporter proteins (GLUT family) shows a distinct pattern in the presence of cancer. In malignant cells such as head and neck squamous cell carcinoma, the expression of GLUT1- and GLUT3-proteins is up-regulated under the activation of hypoxia-inducible factor 1 (HIF-1) in low oxygen concentration [20]. GLUT-3 has been reported to have both a higher affinity for glucose and at least a five-fold greater transport capacity compared to GLUT-1 [21]. In inflammatory tissue, which may be abundant in white blood cells such as lymphocytes, monocytes, macrophages, and neutrophils, glucose transport is more similar to healthy tissue in spite of the presence of GLUT-3 [22]. Second, the preference of malignant cells for glycolysis as opposed to the respiration of normal cells results in metabolic features potentially detectable at long or delayed imaging protocols.

The idea of the evaluation of temporal changes in [^{18}F]-FDG uptake to improve specificity has been utilized in some previous studies. Among them, dual-time point imaging is the most common investigated acquisition protocol. Several studies have been performed in non-small-cell lung

cancer to evaluate this method in the distinction of mediastinal lymph node metastases from inflammatory changes, but the results have been controversial [23,24]. Indeed, a recent meta-analytic comparison between single and dual-time point imaging in a variety of solid tumours found the latter to be more sensitive but less specific in the evaluation of metastatic nodal involvement and did not support the routine use of dual-time point [^{18}F]-FDG PET/CT for the diagnosis of metastatic lymph nodes [25].

In the recent years several computational methods have been proposed to be used in medical image registration and segmentation [26,27,28] Moreover, classification algorithms have been used widely as segmentation algorithms for medical images [29]. Based on our previous experience [30], we adopted two well-characterized clustering algorithms, GMM and K-means, for management of the data of the current study. Our main hypothesis was that the dynamic features could better differentiate tissues compared to the static parameter SUV. The features were calculated from dynamic data of the VOIs in PET/CT images, which required much longer acquisition protocol compared to that in the standard planning of RT. All seven features (D1-D7) were then evaluated with the two algorithms.

First, the tracer retention index (D1) showed a favorable capability to distinguish between tumour and healthy tissue VOI in this study population. D1 resembles retention indices reported in dual-time point protocols, although we used the initial 10 frames (0-10 min from injection) rather than the much later 45-60 min. window typical of several previous studies to calculate the first time point [23, 24, 31]. In spite of the wide range of the D1 of our tumour VOIs, there was no overlap with the healthy tissue VOIs. On the other hand, voxel-wise analyses using clustering algorithms showed only moderately low specificity for D1 in the distinction of healthy tissue and tumour voxels. This is probably due to the manual contouring of the tumour volume, which tends to be done by oversegmenting the tumour in order to avoid a geographic miss in RT.

Second, the patients with tonsillar carcinoma had lower [^{18}F]-FDG uptake as well as retention index (D1) in their tumour VOIs compared to the patients with non-tonsillar carcinoma. The shape of the tumour TACs in tonsillar carcinoma was different from that of non-tonsillar carcinoma (Fig. 2 and 3) and did not exhibit the usual steep rising curve of malignant tumours [32]. Our observation needs to be considered as preliminary owing to the small number of cases, but it clearly warrants future investigation of similar patients.

The analysis of discrimination of primary tumour and inflammation voxels showed that dynamic feature D3 provided a little better performance compared to the static parameter SUV. The feature D3 is the area under the TAC between the 20th and the 21st PET frames (30-70 minutes). D6 (temporal variance) represents the total change in the radioactivity concentration over the entire period of time, and this feature explains how quickly the signal becomes stable. Among non-tonsillar carcinoma patients, the features D1 and D6 showed also slightly higher specificity and sensitivity compared to the SUV. These three features can rationally be considered to represent the potential differences between glucose transport and the metabolism of different tissue types, although the biological background behind these findings remains obscure.

Variance of local change (D5) is a unique feature, since it is not dependent on the tracer uptake rate. Instead, D5 describes the in-flux and out-flux of glucose through the cell membranes and thus is analogous to the ratio of rate constants K_1 and k_2 of the original Sokoloff equation describing [^{18}F]-FDG kinetics in dynamic PET studies [33]. Nonetheless, this theoretical background of the feature did not provide a reasonable explanation for the slightly superior performance of D5 compared to

SUV in the discrimination of primary tumour and metastatic lymph node observed in this study population. Furthermore, unlike in the SUV, we do not know the repeatability of D5 over sequential scans performed within a short time span.

Some of the dynamic features showed different specificity and sensitivity with the K-means algorithm as compared to the calculations with GMM algorithm. The higher sensitivity and specificity obtained with the K-means algorithm may be explained by the fact that K-means can better classify into separate groups data which does not show normal distribution. On the other hand, the GMM algorithm outperformed K-means in some calculations, which indicates that neither of the algorithms can be regarded as preferable in every situation. This may be due to the fact that GMM utilizes the expectation maximization algorithm, which estimates the maximum likelihood of the data point belonging to either of the classes. With a larger study population it might be valuable to perform also further analyses by combining several dynamic features in the distinction of different tissue types. Intuitively it might be beneficial to take into account the individual features of glucose metabolism and transport in different tissue types when considering how to combine the features for separate analyses.

In this study, the patients fasted four hours before [^{18}F]-FDG PET/CT-imaging, but the blood glucose level was not monitored before the imaging session. This can be considered as a weakness of the study protocol. On the other hand, none of our patients had any history of diabetes or impaired glucose tolerance, and the retrospective review of hospital charts did not reveal any suspicion of abnormal glucose metabolism during the cancer treatment and follow-up period. None of the study subjects was obese (body mass index >30 kg/m^2) and none of them had any medication (e.g. systemic corticosteroid) likely to cause a temporary change in glucose metabolism. Therefore it is very unlike that any of the patients would have had a high plasma glucose level (>11.0 mmol/l) during the imaging.

Finally, we have to consider how our approach could be implemented in the workflow of a busy RT department. The dynamic acquisition takes longer than standard static imaging, and longer sessions are uncomfortable for patients, since they have to wear a thermoplastic mask during the imaging. A clear advantage compared to classical dynamic studies evaluating [^{18}F]-FDG kinetics is the lack of measurement of input function, which removes the need for extracting blood from the patient during acquisition. In this study, the imaging procedure was well tolerated, but our patients had good performance, and this kind of imaging protocol would be very challenging for tracheostomized patients or patients requiring a mouth bite for immobilization during the imaging session.

Conclusions

We found in this small pilot study that some dynamic features obtained by the extended PET/CT acquisition showed slightly superior performance compared to the SUV for differentiation of tumour from normal and inflammatory tissues in oropharyngeal cancer. The improvement in specificity and sensitivity was modest, and a large variation was seen for all features. This rules out any clear or statistically significant conclusion on the clinical value of any of the tested dynamic features of their relative discrimination capability compared with SUV, and is due in part to the difficulty in recruiting a large enough cohort of subjects with similar pathology. Some of these features may, however, provide additional information compared to static imaging, and we encourage further study of dynamic features in fit patients who tolerate the discomfort resulting from longer-than-standard imaging protocols.

Acknowledgements

We thank Rikard Owenius, PhD for our ability to learn from each other in this and a related project. We also thank the staff at Turku PET Centre and the Department of Oncology and Radiotherapy in Turku University Hospital. This study was supported in part by the Cancer Foundation in Finland, Hospital District of Southwest Finland, and the National Graduate School of Clinical Investigation.

Conflicts of interest

Antti Silvoniemi, Mueez U Din, Sami Suilamo, Tony Shepherd and Heikki Minn declare that they have no conflict of interest.

References

1. Marur S, Burtness B (2014) Oropharyngeal squamous cell carcinoma treatment: current standards and future directions. Curr Opin Oncol 26:252-258
2. Lee MK, Nalliah RP, Kim MK, Elangovan S, Allareddy V, Kumar-Gajendrareddy P, Allareddy V (2011) Prevalence and impact of complications on outcomes in patients hospitalized for oral and oropharyngeal cancer treatment. Oral Surg Oral Med Oral Pathol Oral Radiol Endod 5:581-591
3. Nguyen NP, Vos P, Smith HJ, Nguyen PD, Alfieri A, Karlsson U, Dutta S, Lemanski C, Nguyen LM, Sallah S (2007) Concurrent chemoradiation for locally advanced oropharyngeal cancer. Am J Otolaryngol 28:3-8
4. Guido A, Fuccio L, Rombi B, Castellucci P, Cecconi A, Bunkheila F, Fuccio C, Spezi E, Angelini AL, Barbieri E (2009) Combined 18F-FDG-PET/CT imaging in radiotherapy target delineation for head-and-neck cancer. Int J Radiat Oncol Biol Phys 73:759-763
5. Minn H, Suilamo S, Seppälä J (2010) Impact of PET/CT on planning of radiotherapy in head and neck cancer. Q J Nucl Med Mol Imaging 54:521-532
6. Hammarstedt L, Lindquist D, Dahlstrand H, Romanitan M, Dahlgren LO, Joneberg J, Creson N, Lindholm J, Ye W, Dalianis T, Munck-Wikland E (2006) Human papillomavirus as a risk factor for the increase in incidence of tonsillar cancer. Int J Cancer 119:2620-2623
7. Attner P, Du J, Näsman A, Hammarstedt L, Ramqvist T, Lindholm J, Marklund L, Dalianis T, Munck-Wikland E (2010) The role of human papillomavirus in the increased incidence of base of tongue cancer. Int J Cancer 126:2879-2884
8. Chaturvedi AK, Engels EA, Pfeiffer RM, Hernandez BY, Xiao W, Kim E, Jiang B, Goodman MT, Sibug-Saber M, Cozen W, Liu L, Lynch CF, Wentzensen N, Jordan RC, Altekruse S, Anderson WF, Rosenberg PS, Gillison ML (2011) Human papillomavirus and rising oropharyngeal cancer incidence in the United States. J Clin Oncol 29:4294-4301
9. Ang KK, Harris J, Wheeler R, Weber R, Rosenthal DI, Nguyen-Tân PF, Westra WH, Chung CH, Jordan RC, Lu C, Kim H, Axelrod R, Silverman CC, Redmond KP, Gillison ML (2010) Human papillomavirus and survival of patients with oropharyngeal cancer. N Engl J Med 363:24-35
10. Dalianis T (2014) Human papillomavirus and oropharyngeal cancer, the epidemics, and significance of additional clinical biomarkers for prediction of response to therapy (Review). Int J Oncol 44:1799-1805
11. Masterson L, Moualed D, Liu ZW, Howard JE, Dwivedi RC, Tysome JR, Benson R, Sterling JC, Sudhoff H, Jani P, Goon PK (2014) De-escalation treatment protocols for human papillomavirus-associated oropharyngeal squamous cell carcinoma: a systematic review and meta-analysis of current clinical trials. Eur J Cancer 50:2636-2648
12. Metser U, Even-Sapir E (2007) Increased (18)F-fluorodeoxyglucose uptake in benign, nonphysiologic lesions found on whole-body positron emission tomography/computed tomography (PET/CT): accumulated data from four years of experience with PET/CT. Semin Nucl Med 37:206-222
13. Muzi M, O´Sullivan F, Mankoff DA, Doot RK, Pierce LA, Kurland BF, Linden HM, Kinahan PE (2012) Quantitative assessment of dynamic PET imaging data in cancer imaging. Magn Reson Imaging 30:1203-1215
14. Carlson ER, Schaefferkoetter J, Townsend D, McCoy JM, Campbell PD Jr, Long M (2013) The use of multiple time point dynamic positron emission tomography/computed

tomography in patients with oral/head and neck cancer does not predictably identify metastatic lymph nodes. J Oral Maxillofac Surg 71:162-177
15. Lassen P, Primdahl H, Johansen J, Kristensen CA, Andersen E, Andersen LJ, Evensen JF, Eriksen JG, Overgaard J (2014) Danish Head and Neck Cancer Group (DAHANCA). Impact of HPV-associated p16-expression on radiotherapy outcome in advanced oropharynx and non-oropharynx cancer. Radiother Oncol 113:310-316
16. Din M. (2014) Differentiation of metabolically distinct areas within head and neck region using dynamic ^{18}F-FDG positron emission tomography imaging. Masters Thesis, University of Turku, available on-line http://urn.fi/URN:NBN:fi-fe201401281303.
17. Ang KK, Garden AS (2012) Radiotherapy for head and neck cancers: indications and techniques, 4th edition. Lippincott Williams & Wilkins, Philadelphia, USA
18. Bonner JA, Harari PM, Giralt J, Azarnia N, Shin DM, Cohen RB, Jones CU, Sur R, Raben D, Jassem J, Ove R, Kies MS, Baselga J, Youssoufian H, Amellal N, Rowinsky EK, Ang KK (2006) Radiotherapy plus cetuximab for squamous-cell carcinoma of the head and neck. N Engl J Med 354:567-578
19. Maldonado A, González-Alenda FJ, Alonso M, Sierra JM (2007) PET-CT in clinical oncology. Clin Transl Oncol 9:494-505
20. Semenza GL (2010) HIF-1: upstream and downstream of cancer metabolism. Curr Opin Genet Dev 20:51-56
21. Simpson IA, Dwyer D, Malide D, Moley KH, Travis A, Vannucci SJ (2008) The facilitative glucose transporter GLUT3: 20 years of distinction. Am J Physiol Endocrinol Metab 295:E242-253
22. Calvo MB, Figueroa A, Pulido EG, Campelo RG, Aparicio LA (2010) Potential role of sugar transporters in cancer and their relationship with anticancer therapy. Int J Endocrinol Epub Jul 18
23. Barger RL Jr, Nandalur KR (2012) Diagnostic performance of dual-time ^{18}F-FDG PET in the diagnosis of pulmonary nodules: a meta-analysis. Acad Radiol 19:153-158
24. Schillaci O (2012) Use of dual-point fluorodeoxyglucose imaging to enhance sensitivity and specificity. Semin Nucl Med 42:267-280
25. Shen G, Deng H, Hu S, Jia Z (2014) Potential performance of dual-time-point ^{18}F-FDG PET/CT compared with single-time-point imaging for differential diagnosis of metastatic lymph nodes: a meta-analysis. Nucl Med Commun 35:1003-1010
26. Tavares JM (2014) Analysis of biomedical images based on automated methods of image registration. In: Bebis G et al (Ed) Advances in visual computing, 1st edn, Springer International Publishing, Switzerland, pp 21-30
27. Alves RS, Tavares JM (2015) Computer image registration techniques applied to nuclear medicine images . In: Tavares JM et al (Ed) Computational and experimental biomedical sciences: methods and applications, 1st edn, Springer International Publishing, Switzerland, pp 173-191
28. Oliveira FP, Borges Faria D, Campos Costa D, Tavares JM (2014) A robust computational solution for automated quantification of a specific binding ratio based on [123I]FP-CIT SPECT images. Q J Nucl Med Mol Imaging 58:74-84
29. Ma Z, Tavares JM, Jorge RN, Mascarenhas T (2010) A review of algorithms for medical image segmentation and their applications to the female pelvic cavity. Comput Methods Biomech Biomed Engin 13:235-246
30. Shepherd T, Owenius R (2012) Gaussian process models of dynamic PET for functional volume definition in radiation oncology. IEEE Trans Med Imaging 31:1542-56

31. Abgral R, Le Roux Py, Rousset J, Querellou S, Valette G, Nowak E, Turzo A, Tissot V, Marianowski R, Salaün PY (2013) Prognostic value of dual-time-point 18F-FDG PET/CT-imaging in patients with head and neck squamous cell carcinoma. Nucl Med Commun 34:551-556
32. Sakamoto H, Nakai Y, Ohashi Y, Okamura T, Ochi H (1997) Positron emission tomographic imaging of head and neck lesions. Eur Arch Otorhinolaryngol 254:Suppl1:S123-126
33. Minn H, Zasadny KR, Quint LE, Wahl RL (1995) Lung cancer: reproducibility of quantitative measurements for evaluating 2-[F-18]-fluoro-2-deoxy-D-glucose uptake at PET. Radiology 196:167-173

Figure Legends:

Fig. 1 Dynamic PET/CT acquisition protocol

Fig. 2 Time-activity curves of volumes of interests of patients nr 1-3 with HPV-positive tonsillar carcinoma (black=primary tumour, orange=healthy tissue, blue=metastatic lymph node, red=inflammatory region left side, green=inflammatory region right side)

Fig. 3 Time-activity curves of volumes of interests of patients with HPV-positive (nr 4) and HPV-negative (nr 5) non-tonsillar carcinoma (black=primary tumour, orange=healthy tissue, blue=metastatic lymph node, red=inflammatory region left side, green=inflammatory region right side)

Fig. 4 PET/CT images of patient nr 3. The primary tumour is located in the right palatine tonsil and the metastatic lymph node is located on the right side of the neck (a). The dental inflammatory lesions on both sides of the mandible are visible (b)

Table 1 Characteristics and clinical data of the patients

Patient nr	Age (years)	Weight (kg)	Tumour location	TNM-classification	Stage	Grade	p16 staining	Injected activity (MBq)	Clinical outcome 2 years after primary treatment
1	63	79	tonsil	T2N2BM0	IVA	III	+	320	progressive disease †
2	65	74	tonsil	T3N2BM0	IVA	II	+	309	remission
3	59	80	tonsil	T2N2BM0	IVA	II	+	298	remission
4	59	88	base of tongue	T3N2BM0	IVA	II	+	294	progressive disease
5	58	63	orophrayngeal wall	T3N0M0	III	I	-	284	progressive disease †

The tumour stage is given according to the guidelines of the International Union Against Cancer (UICC). († = dead of disease).

Table 2 List of dynamic features utilized in the analyses of the study

"A" refers to the activity concentration and "T" to the time of PET frame. The corresponding PET frame is presented with the number in the subscript. The subscript "early" refers to the first ten PET frames and the subscript "late" to the 21st PET frame.

Dynamic feature	**Description**	**Equation**
D1	Retention index	Retention index = $(A_{late}-A_{early})/A_{early}$
D2	Early slope	Early slope= (mean($A_{15,}A_{16}…A_{20}$)-mean($A_{1,}A_{2}…A_{10}$))/(mean($T_{15,}T_{16}...T_{20}$)-mean($T_1,T_2…T_{10}$))
D3	Area under the TAC_{20-21}	Area under the TAC_{20-21}= (($T_{21}-T_{20}$)x($A_{21}-A_{20}$)/2)+($T_{21}-T_{20}$)xA_{20}
D4	Sum Fluctuation 1-22	Sum $fluctuation_{1-22}$= $\|A_2-A_1\|+\|A_3-A_2\|+\|A_4-A_3\|….+\|A_{22}-A_{21}\|$
D5	Variance of local change	Variance of local change = Var[(A_2-A_1),(A_3-A_2)…($A_{22}-A_{21}$)]
D6	Temporal variance	Temporal variance = Var[$A_1,A_2,A_3…A_{22}$]
D7	Sum of three slopes	Sum of three slopes = Slope 1 + Slope 2 + Slope 3 where, Slope 1= (mean($A_{15},A_{16}…A_{20}$)-max($A_1,A_2…A_5$))/(mean($T_{15},T_{16}…T_{20}$)-max(T_A)) Slope 2=($A_{21}-A_{20}$)/($T_{21}-T_{20}$) Slope 3 =($A_{22}-A_{21}$)/($T_{22}-T_{21}$)

Table 3 Mean standardized uptake values (SUV) of volumes of interests

Patient nr	Primary tumour	Metastatic lymph node	Inflammatory lesion left	Inflammatory lesion right	Healthy tissue
1	2.08	2.95	4.33	4.29	1.51
2	2.56	3.07	3.94	2.88	1.73
3	2.62	2.11	3.76	4.41	1.28
4	7.32	4.73	NA	3.82	1.98
5	5.61	NA	2.35	NA	1.36
Median	2.62	3.01	3.85	4.06	1.51

Table 4 Performance of SUV and dynamic features in discrimination of voxel of different tissue types. *) The results of GMM-classification are presented as area under the curve (AUC) from ROC analysis, where a value of 1.0 signifies the best possible discrimination. The results of K-means classification are presented as sensitivity/specificity, also in the range 0 to 1.0. Values in bold reveal where dynamic features perform better than SUV in classification.

Volumes of interest in discrimination	**Algorithm* G=GMM K=K-MEANS**	**SUV**	**D1**	**D2**	**D3**	**D4**	**D5**	**D6**	**D7**
Primary tumour and inflammation (all patients)	G	0.825	0.812	0.707	**0.845**	0.703	0.689	0.764	0.801
Primary tumour and inflammation (all patients)	K	0.723/ 0.896	0.645/ 0.877	0.667/ 0.631	0.691/ 0.929	0.592/ 0.713	0.556/ 0.726	0.600/ 0.405	0.629/ 0.704
Primary tumour and inflammation (tonsillar ca)	G	0.864	0.799	0.726	**0.870**	0.678	0.684	0.738	0.828
Primary tumour and inflammation (tonsillar ca)	K	0.811/ 0.861	0.685/ 0.836	0.741/ 0.507	0.765/ 0.905	0.606/ 0.651	0.595/ 0.690	0.629/ 0.373	0.688/ 0.606
Primary tumour and inflammation (non-tonsillar ca)	G	0.706	**0.853**	0.650	**0.771**	**0.776**	0.702	**0.840**	**0.721**
Primary tumour and inflammation (non-tonsillar ca)	K	0.458/ 1.000	**0.522/ 1.000**	0.447/ 1.000	**0.468/ 1.000**	0.550/ 0.900	0.437/ 0.833	0.512/ 0.500	0.451/ 1.000
Primary tumour and healthy tissue (all patients)	G	0.879	0.760	0.710	0.827	0.690	0.690	0.675	0.673
Primary tumour and healthy tissue (all patients)	K	0.624/ 0.932	0.641/ 0.725	0.519/ 0.428	0.580/ 0.778	0.525/ 0.669	0.462/ 0.835	0.358/ 0.763	0.523/ 0.711
Metastatic lymph node and primary tumour (all patients)	G	0.669	0.642	0.651	0.641	0.648	0.594	0.654	0.650
Metastatic lymph node and primary tumour (all patients)	K	0.291/ 0.716	0.294/ 0.610	0.475/ 0.613	0.302/ 0.707	0.560/ 0.713	**0.329/ 0.842**	0.131/ 0.867	0.230/ 0.605
Metastatic lymph node and inflammation (all patients)	G	0.783	0.623	0.681	0.763	0.704	0.727	0.678	0.568
Metastatic lymph node and inflammation (all patients)	K	0.791/ 0.630	0.598/ 0.519	0.498/ 0.565	0.765/ 0.639	0.638/ 0.542	0.397/ 0.756	0.469/ 0.604	0.669/ 0.461

Fig. 1

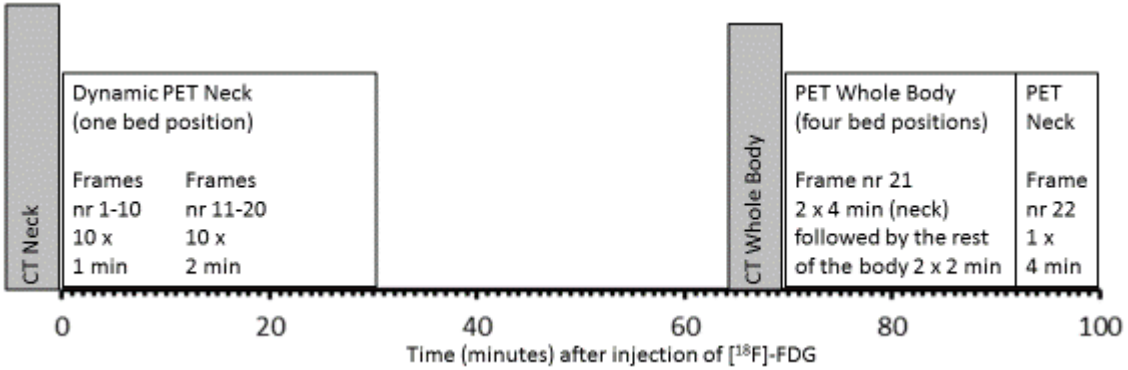
CT Neck
Dynamic PET Neck
(one bed position)
Frames
nr 1-10
10 x
1 min
Frames
nr 11-20
10 x
2 min
CT Whole Body
PET Whole Body
(four bed positions)
Frame nr 21
2 x 4 min (neck)
followed by the rest
of the body 2 x 2 min
PET
Neck
Frame
nr 22
1 x
4 min
0
20
40
60
80
100
Time (minutes) after injection of [18F]-FDG

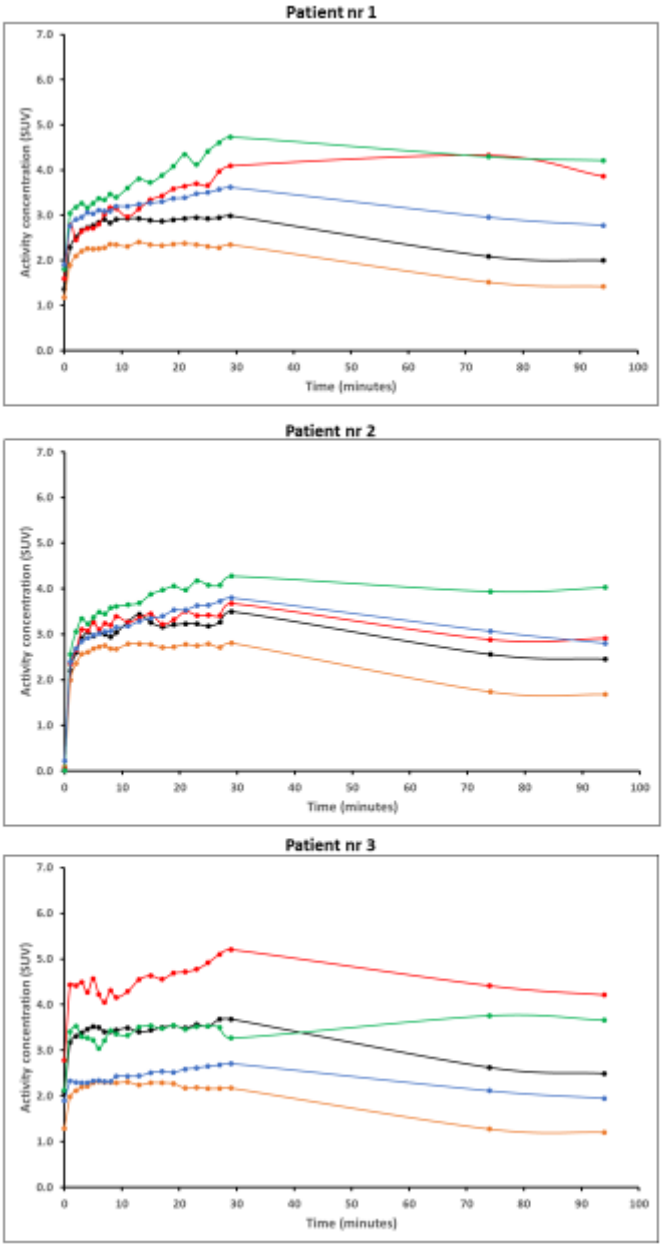
Patient nr 1
Activity concentration (SUV)
Time (minutes)
Patient nr 2
Activity concentration (SUV)
Time (minutes)
Patient nr 3
Activity concentration (SUV)
Time (minutes)

Fig. 2

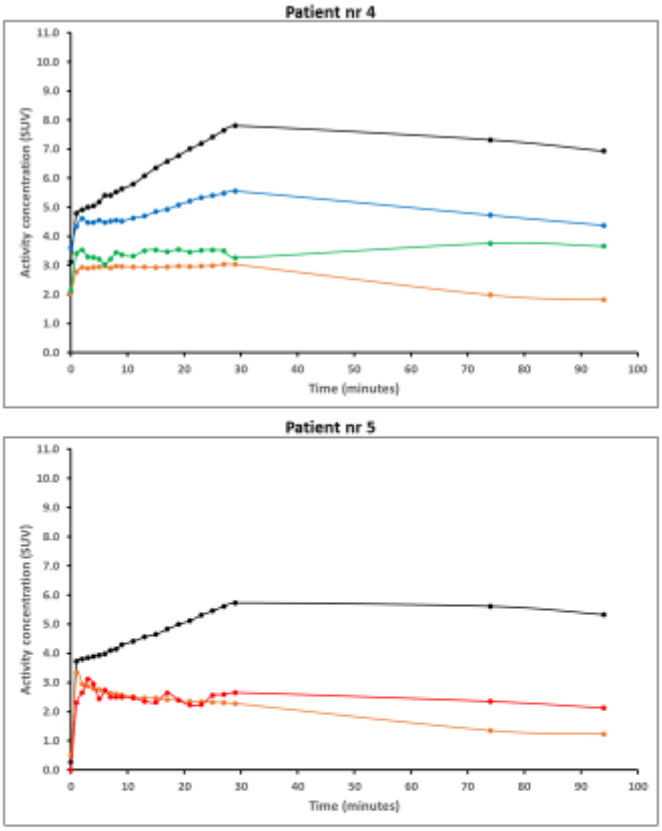
Patient nr 4
Activity concentration (SUV)
Time (minutes)
Patient nr 5
Activity concentration (SUV)
Time (minutes)

Fig. 3

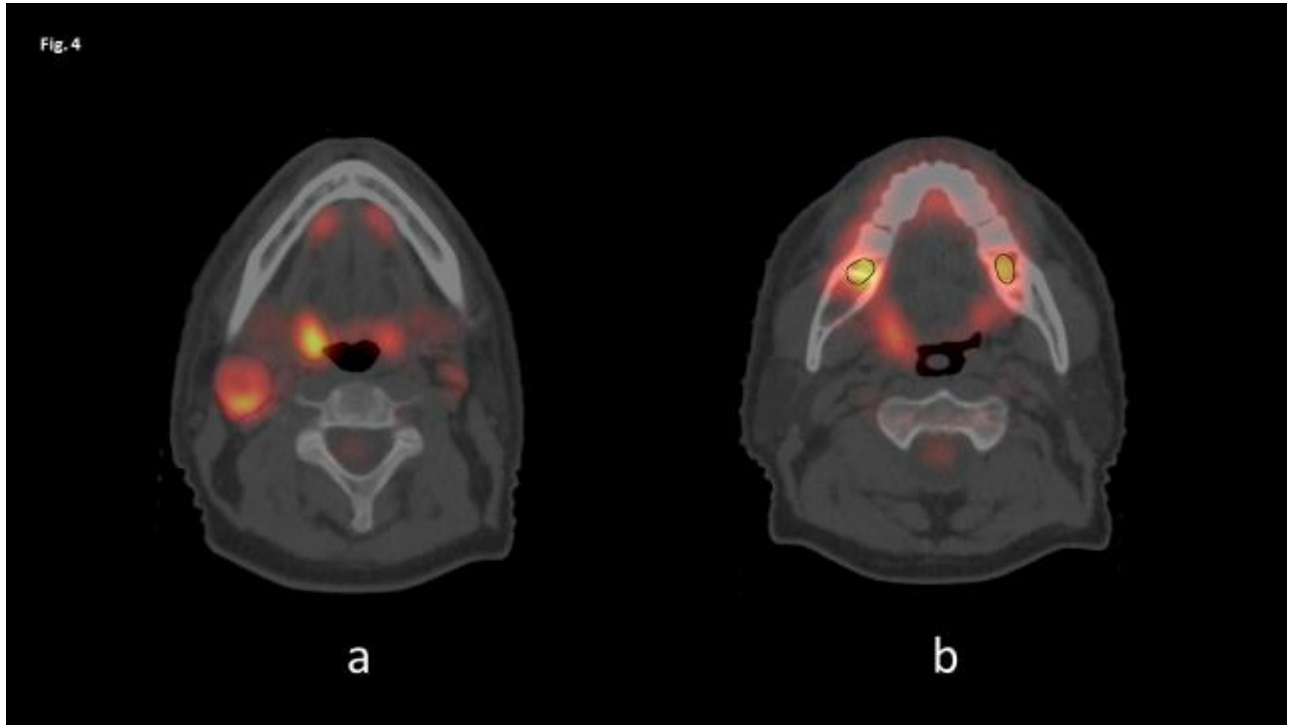
Fig. 4
a
b